HHS Public Access

Author manuscript

J Mater Sci Mater Med. Author manuscript; available in PMC 2019 June 30.

Published in final edited form as:

J Mater Sci Mater Med. ; 29(5): 58. doi:10.1007/s10856-018-6052-6.

A novel synthetic route for high-index faceted iron oxide concave nanocubes with high T_2 relaxivity for *in vivo* MRI applications

Shu F. Situ-Loewenstein[1], **Sameera Wickramasinghe**[1], **Eric C. Abenojar**[1], **Bernadette O. Erokwu**[2], **Chris A. Flask**[2,3,4], **Zhenghong Lee**[2], and **Anna Cristina S. Samia**[1]

[1]Department of Chemistry, Case Western Reserve University, 10900 Euclid Avenue, Cleveland, OH 44106, USA

[2]Department of Radiology, Case Western Reserve University, 10900 Euclid Avenue, Cleveland, OH 44106, USA

[3]Department of Biomedical Engineering, Case Western Reserve University, 10900 Euclid Avenue, Cleveland, OH 44106, USA

[4]Department of Pediatrics, Case Western Reserve University, 10900 Euclid Avenue, Cleveland, OH 44106, USA

Abstract

Iron oxide nanoparticles (IONPs) with high-index facets have shown great potential as high performance T_2 contrast agents for MRI. Previous synthetic approaches focused mainly on ion-directed or oxidative etching methods. Herein, we report a new synthetic route for preparing high-index faceted iron oxide concave nanocubes using a bulky coordinating solvent. Through the systematic replacement of a non-coordinating solvent, 1-octadecene, with trioctylamine, the solvent interaction with the nanoparticle surface is modified, thereby, promoting the growth evolution of the IONPs from spherical to concave cubic morphology. The presence of the bulky trioctylamine solvent results in particle size increase and the formation of nanoparticles with enhanced shape anisotropy. A well-defined concave nanocube structure was evident from the early stages of particle growth, further confirming the important role of bulky coordinating solvents in nanoparticle structural development. The unique concave nanocube morphology has a direct influence on the magnetic properties of the IONPs, ultimately leading to an ultra-high T_2 relaxivity (862.2 mM^{-1} s^{-1}), and a 2-fold enhancement in T_2*-weighted *in vivo* MRI contrast compared to spherical IONP analogs.

Graphical Abstarct

Anna Cristina S. Samia, anna.samia@case.edu.

Conflict of interest The authors declare that they have no conflict of interest.

Electronic supplementary material The online version of this article (https://doi.org/10.1007/s10856-018-6052-6) contains supplementary material, which is available to authorized users.

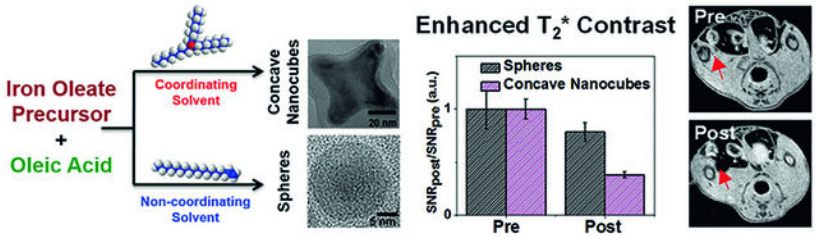

1 Introduction

IONPs are commonly used as T_2 contrast agents in MRI due to their unique magnetic properties and biocompatibility [1–5]. While chemical composition tuning has been demonstrated to be an effective route to improve the magnetic properties of IONPs for enhanced spin-spin (T_2) relaxation [2], inducing shape anisotropy has also been shown to improve imaging contrast in MRI applications [1]. Zhao et al. have recently synthesized octapod-shaped IONPs with high transverse relaxivity (r_2) values in the 680 mM^{-1} s^{-1} range [6]. The intrinsic magnetic properties of IONPs are strongly correlated to the relaxation properties [4–6], and improved T_2 relaxation has been previously attributed not only to the increase in the local magnetization field during MRI measurements, but also to the expanded effective radius of the local field, and the increase in magnetic field inhomogeneity upon using high-index faceted IONP contrast agents [6–9].

To date, various synthetic methods have been developed to prepare IONPs and the thermal decomposition approach is highly regarded for its ability to produce high quality IONPs with controllable sizes and tunable morphologies [10–13]. Several groups have investigated the effects of changing various reaction parameters on the NP's structural growth [12–15]. Chemical additives have been explored to induce the formation of high-index faceted nanostructures through selective capping of the nanoparticle surface [6, 16–20]. Hematite (α-Fe_2O_3) concave nanocubes with an average size of 300 nm have been synthesized in the presence of cupric acetate under hydrothermal conditions [16]. During the synthesis process, the Cu^{2+} ions acted as facet-selective capping agents and were demonstrated to be responsible for promoting the concave surface nanostructure. Similar to metal ions, Cl^- ions have also been shown to be effective selective capping agents in creating shape anisotropic IONPs [6]. On the other hand, exposure to air during IONP synthesis has also been demonstrated to induce oxidative etching to create negative surface curvatures in concave nanocubes [21].

Aside from the investigations of the structural modifications on IONPs through the introduction of additives, previous studies have also explored the effects of other synthetic parameters on the resulting NP morphology [15, 22–27]. Oleic acid is a common capping ligand used in the synthesis of high quality IONPs due to its ability to strongly bind to the NP surface through its carboxylate group [23]. Replacing oleic acid with other capping ligands containing weaker binding and/or bulkier molecular structures, such as oleylamine, 1,2-hexadecanediol, and trioctylphosphine oxide, have been shown to favor the formation of shape anisotropic IONPs [23–26]. In addition, changing the reaction solvent has also

provided a means to control the growth of IONPs [12]. Typically, a high boiling point solvent such as 1-octadecene (ODE) is used to produce monodisperse IONPs with controllable sizes [12]. While it has been reported that the use of the non-coordinating ODE solvent in the presence of the strongly binding oleic acid ligand during IONP synthesis promotes isotropic spherical morphology, on the other hand, the role of coordinating solvents on the growth of highly faceted IONPs to our knowledge has not been thoroughly investigated yet. Herein, we report a systematic study of the effect of a bulky coordinating solvent, trioctylamine (TOA), on the morphological formation of high-index faceted concave nano-cube IONPs. Moreover, to better understand how each synthetic condition contributes toward the formation of a concave cubic IONP nanostructure, we studied the effects of differently prepared iron oleate precursors, reflux temperature, ligand ratio, and different solvent types on the morphology of IONPs prepared through the thermal decomposition method. The resulting concave nanocubes synthesized using TOA as solvent were evaluated to have an ultra-high T_2 relaxivity, and exhibited a 2-fold enhancement in T_2*-weighted *in vivo* MRI contrast compared to spherical IONP analogs.

2 Materials and methods

2.1 Materials

Iron (III) chloride hexahydrate (98%), oleic acid (90%), 1-octadecene (90%), trioctylamine (98%), trimethylamine N-oxide (98%), polysorbate-80, and toluene were purchased from Sigma-Aldrich and used as received. Hexane, sodium oleate, ethyl alcohol, and sodium chloride were purchased from Fisher Scientific and were used without further purification.

2.2 Synthesis of the iron oleate precursor

The iron oleate precursor was prepared by dissolving iron(III) chloride hexahydrate ($FeCl_3.6H_2O$) and sodium oleate in a solvent mixture containing deionized (DI) water, ethanol, and hexane (3:4:7 volume ratio). The reaction mixture was heated at reflux for 4 h. After reflux, the organic layer containing the iron oleate precursor was separated from the aqueous layer. Three additional extraction cycles were performed on the organic portion with warm water to remove NaCl by-product and excess reagents. Following the wash steps, the iron oleate precursor was allowed to dry inside of a fume hood until a waxy paste was obtained.

2.3 Synthesis of the IONPs

Using the previously synthesized iron oleate precursor, the IONPs were prepared by a modified thermal decomposition method [12]. Specifically, the iron oleate precursor (1.8 g, 2.0 mmol) and oleic acid ligand (1.8 ml, 5.1 mmol) were dissolved in trioctylamine/1-octadecene (12.5 ml) under vigorous stirring in an inert atmosphere (Ar gas). The reaction mixture was then heated to 100 °C at a rate of 3.3 ° C/min and held at that temperature for 1 h, after which the temperature was again increased to reflux temperature and held for an additional hour. The reaction mixture was then cooled to room temperature and the nanoparticles were isolated by centrifugation for 20 min at 7000 rpm using a 1:1 ethanol: toluene solvent wash mixture. The as-synthesized nanoparticles were in wüstite (FeO) phase and thus, the FeO NPs were converted to the magnetite (Fe_3O_4)phase using trimethylamine

N-oxide $(CH_3)_3NO$ as oxidizing agent. More specifically, 0.5 mmol of $(CH_3)_3NO$ was added to 5.6 mmol of FeO nanoparticles dispersed in 20 ml of 1-octadecene and the reaction mixture was first heated to 130 °C and held for 1 h, after which the reaction temperature was raised to 280 °C at a rate of 10 °C/min and held at that temperature for 1 h.

2.4 Phase transfer of Fe_3O_4 NPs

The Fe_3O_4 NPs were phase-transferred in water by encapsulating with polysorbate-80. Specifically, 5 mg of the nanoparticles in toluene were first dried under vacuum and re-dispersed in tetrahydrofuran (THF) via sonication, followed by the addition of 100 μl of polysorbate-80. The sample was then left to mix in a rotor overnight, centrifuged at 8500 rpm for 30 min, and re-dispersed in DI water for the succeeding MRI studies.

2.5 Characterization

The size and shape of the IONPs were evaluated by transmission electron microscopy (TEM). TEM samples were prepared by placing 5 μl of a dilute suspension of the nanoparticles on a 400 mesh Formvar-coated copper grid and allowing the solvent to evaporate slowly at room temperature. TEM images were obtained with a FEI Tecnai G2 Spirit BioTWIN transmission electron microscope operated at 120 kV. The mean particle size and size distribution were evaluated by measuring at least 200 nanoparticles for each sample. The tilted TEM images were acquired using a FEI Tecnai TF30 ST instrument operated at 300 kV.

The Fourier-transform infrared (FTIR) spectra of the iron oleate precursor were obtained with a JASCO™ FTIR-4600 spectrometer in the mid IR range from 600 to 4000 cm^{-1}. The same iron oleate precursor deposited on a silicon wafer was further analyzed with a Bruker Sentinel Raman spectrometer in the spectral range of 290 to 1700 cm^{-1} and the data was processed with GRAMS32/AI™ spectroscopy software.

The crystal phase of the IONP samples were analyzed by powder X-ray diffractometry (PXRD) performed in a Rigaku MiniFlex powder X-ray diffractometer using Cu-Kα radiation ($\lambda = 0.154$ nm). For the XRD analyses, the diffraction patterns were collected within a 2–θ range of 25 to 75°. The field-dependent magnetic characterization of the oxidized Fe_3O_4 IONPs was performed using a Quantum Design MPMS5 Superconducting Quantum Interference Device (SQUID) magnetometer. The field-dependent magnetic properties of the Fe_3O_4 NP samples were obtained at 300 K from −5 to 5 T.

The total Fe concentration in each IONP sample was measured using a fast sequential atomic absorption spectrophotometer (AAS) Varian 220FS AA. For the elemental Fe analysis, the samples were digested with concentrated hydrochloric acid (37%) overnight to completely dissolve the IONPs. The average hydrodynamic radii of the phase-transferred IONP samples were measured by dynamic light scattering (DLS) on a ZetaPALS particle size analyzer (Brookhaven) at a scattering angle of 90°.

2.6 Relaxivity measurements

The relaxivity of the series of phase-transferred IONPs was measured on a 1.5 T 60 MHz Bruker minispec NMR relaxometer. The T_2 relaxation times were recorded in water at room temperature at the following Fe concentrations (evaluated from AAS) for each of the iron oxide nano-particle samples: 0, 0.025, 0.05, 0.1, and 0.2 mM. The relaxivity value (r_2) was calculated based on the following equation:

$$\frac{1}{T_{2_{sample}}} = \frac{1}{T_{2_{solvent}}} + r_2[M]$$

2.7 *In vivo* MRI experiments

All the animal work were performed in an AAALAC-approved animal facility at Case Western Reserve University. The experimental protocols have been approved by the CWRU institutional animal care and use committee (IACUC-2015–0123) for this project. In this study, four Charles River CD1-ICR mice were used in the MR imaging experiments in accordance with regulatory guidance on the care and use of the experimental mice. Four adult male CD1-ICR mice (age = 6 weeks, Charles River Labs) were anesthetized and positioned within a mouse MRI volume coil (inner diameter = 35 mm) in a 7 T pre-clinical Bruker Biospec MRI scanner (Bruker Inc., Billerica, MA). Each animal was anesthetized with isoflurane (1–2%) to maintain a respiration rate of 40–60 breaths/minute. Each animal's body temperature was maintained at 35 ± 1 °C with a warmed-air control system. Following initial localizer scans, two sets of high resolution T_2*-weighted FLASH images (Fast Low Angle Shot) were obtained for each mouse: pre-injection as well as 0.5 h post-injection. The axial FLASH scans (TR/TE = 690/3 ms, resolution = 117 × 117 × 500 micron, tip angle = 50 degrees) were obtained with respiratory triggering (SA Instruments, Stony Brook, NY) to limit respiratory motion artifacts. Post-contrast scans were obtained following injection of the mice with the IONP contrast agents (spheres and concave nanocubes at a concentration of 0.3 ml, 2.5 mg Fe/kg of body weight). Injections were made near the abdominal region of the mice and the results were more reflective of an intramuscular injection approach. A direct injection (not an infusion) was preferred in this study because the IONP samples were non-targeted and this method slows down the nanoparticle diffusion leading to a more focused area with higher imaging contrast, which enables the comparison of the two types of IONPs. It was ensured that the animal motion was limited (to avoid IONP diffusion) and the mice were similarly positioned pre- and post-contrast MRI evaluation.

3 Results

3.1 Synthesis of high-index faceted concave cubic IONPs

To investigate solvent effects on the structural evolution of the IONPs, the thermal decomposition of the iron oleate precursor was performed in the presence of oleic acid (OAc) as the capping ligand, and a bulky coordinating solvent, trioctylamine (TOA). The as-synthesized IONPs revealed a clear cubic morphology with negative surface curvature (Fig.

1a, b). The resulting concave cubic IONPs have an average size of 41 nm. To further examine the morphology of the IONPs, TEM images from multiple views (−30°, −15°, 0°, +15°, +30°) were obtained. The collection of the tilted TEM images taken at different viewing angles clearly shows the existence of negative curvature on the surface of the cubic IONPs (Fig. 1c).

3.2 Growth kinetics of high-index faceted concave cubic IONPs

To further investigate the role of TOA on the growth of the concave IONPs, the effect of reflux time on the structural evolution of the concave nanocubes was evaluated by withdrawing aliquots from the reaction mixture at different reflux times for TEM analysis. Immediately at 30 s after reaching the reflux temperature, the IONPs already displayed a distinct concave cubic morphology, and the IONP size and morphology remained unchanged at longer reflux times (Fig. S1), which is consistent with previous reports on other types of high-index faceted NPs synthesized via high-temperature decomposition methods [28].

The presence of a well-defined concave nanocube structure at the early stage of particle growth demonstrated that the formation of the concave cubic morphology was most likely due to the selective binding of TOA on the IONP surface, which is in contrast to the previously reported chemical etching approach where the negative curvature was only observed after longer reaction times [21].

3.3 The effect of iron oleate precursor on the growth of high-index faceted concave cubic IONPs

The reproducibility of a nanoparticle synthetic route is highly appreciated, especially in a system where the conditions are adjusted to form a high-index faceted structure over energetically favored morphologies. During our study, we observed that the level of dryness of the iron oleate precursor plays a critical role on the resulting morphology of the synthesized IONPs. To systematically study the effect of the iron oleate precursor on the nanoparticle growth, the final organic extract of the iron oleate made following the steps described in Section 2.2 was equally divided into two halves and dried in two different methods; one half was dried on a deep container (Method 1) and the other half was dried on a shallow container (Method 2). The two batches of IONPs prepared using the iron oleate precursor from drying Methods 1 and 2, while maintaining other synthetic conditions the same, have turned out to be structurally different (Fig. S2a). The concave shape of the IONPs was well preserved in the product obtained via the precursor dried in Method 2, whereas an intermediate shape (i.e., a structure between perfect cube and concave cube) was obtained from the precursor dried using Method 1.

The intriguing results from TEM analyses led further investigations on the iron oleate precursor obtained from the two drying methods; FTIR and Raman spectroscopy studies were conducted on the iron oleate precursors, as these methods are known to be good analytical tools to study the metal-carboxylate chemistry of iron oleate precursors [18, 29–33]. The FTIR spectra of the iron oleate obtained from two drying methods share four major peaks; 1711 (carbonyl group of free oleic acid or unidentate carboxylate), 1593 (bridging metal-carboxylate), 1524 (bidentate metal-carboxylate), and 1438 (carbonyl group of free

oleic acid) cm^{-1} vibrations (Fig. S2b and S2c). It is evident that both bidentate and bridging metal-carboxylate coordination modes in the precursor obtained from drying Method 1 exist in similar extent whereas, the bridging metal-carboxylate coordination is more pronounced in the precursor obtained from drying Method 2 (area shaded in blue color of Fig. S2c). We assume that this difference in the metal-carboxylate coordination in the iron oleate precursor due to different levels of dryness has been one of the reasons to form the distinct concave cubic structure. Along with FTIR, Raman spectroscopy can also be used to probe the optimal level of dryness of the iron oleate precursor (Fig. S2d). The Raman spectrum of optimally dried iron oleate precursor (Method 2) exhibits peaks at 1270, 1305, 1440 cm^{-1} indicative of the δ(CH) in plane cis olefin group, CH_2 twisting, and CH_2 scissoring of the oleate precursor [34] whereas, the iron oleate precursor from Method 1 was almost featureless in the Raman spectrum.

3.4 The effects of the solvent on the growth of high-index faceted concave cubic IONPs

3.4.1 Coordinating vs. non-coordinating solvent—The importance of having a coordinating solvent in the formation of concave IONPs was tested with a series of IONPs synthesized following the same synthetic conditions(i.e., same amounts of iron oleate precursor and capping ligand, and same heating rate) but, systematically replacing the coordinating solvent, trioctylamine (TOA), with a non-coordinating solvent, 1-ocatadecene (ODE), during the synthesis: (i) 100% TOA, (ii) 20:80% ODE:TOA, (iii) 25:75% ODE:TOA, (iv) 33:67% ODE:TOA, (v) 50:50% ODE:TOA, and (vi) 100% ODE. The concave IONPs synthesized with 100% of TOA as the solvent in synthesis(i) serve as the control experiment (Fig. 2). When 20% of the solvent volume is replaced with the non-coordinating ODE solvent in the synthesis (ii), the structural features of the concave cubes started to diminish. It continuously degraded the concave shape with more ODE solvent replacement during the IONP synthesis (iii), and led to an irregular IONP shape in where ODE served as one third of the total solvent volume, synthesis (iv). Interestingly, the morphology of IONPs clearly shifted from anisotropic structures to isotropic structures after the solvent composition hit the mid-point solvent volume ratios (synthesis v and vi).

3.4.2 Reflux temperature effects—During the change of solvent composition, it is worthy to notice that the average size of the NPs has gradually decreased (Fig. 2), which can be attributed to the decrease in the reflux temperature due the replacement of TOA (b.p. 360 °C) with ODE (b.p. 320 °C). One could argue that not only the chemical properties of the solvent system but, the physical properties such as the reflux temperature are subjected to change from synthesis (i) to (vi), which may have played a role in the final NP morphology. Therefore, we designed an experiment to explore the effect of reflux temperature on the growth of concave IONPs after ruling out changes in chemical composition of the reaction mixture, in which one synthesis was allowed to reflux at 360 °C (control experiment, Fig. S3a) and the other one was held at 320 °C (TOA was used as the only solvent in both syntheses, Fig. S3b). The representative TEM images of the products show that the NPs synthesized at 320 °C remain spherical even if the coordinating solvent, TOA, was used during the synthesis (Fig. S3b). This suggests that the thermal energy given to the system between 320 °C and 360 °C is crucial to differentiate the NP growth stage from the nucleation stage for the concave cubic IONP formation.

3.4.3 Steric effects—The third property of the solvent that influences the formation of the unique concave cubic structure in IONPs is the bulkiness of the coordinating solvent. To investigate steric effects of the solvent during the growth of IONPs, a similar synthesis experiment was conducted ruling out variations in both the chemical nature and physical properties of the reaction mixture components, whereby a primary amine, oleylamine (OAm) was used as the solvent, which has a similar boiling point (364 °C) to TOA. The IONPs synthesized from OAm were also shape anisotropic, but the NPs have irregular shapes (Fig. S4) in contrast to the distinct concave cubic morphology of the IONPs synthesized using TOA as solvent (Fig. S4a). This result demonstrates the important role of a bulky tertiary amine molecular structure in directing the formation of concave nanocube IONPs.

3.5 The effect of the ligand on the growth of high-index faceted concave cubic IONPs

In addition to the effect of the bulky coordinating solvent, the acid-base chemical nature of the ligand and solvent, respectively, can also influence the IONP's morphological development [24]. To examine the role of the oleic acid capping ligand on the formation of the concave cubic IONPs, various amounts of oleic acid were used in the synthesis of the NPs with 100% TOA as solvent. In the absence of oleic acid, the resulting NPs exhibited a sea urchin-like morphology, which is evident at early time points of the reaction (Fig. S5a). At an increased oleic acid concentration (2×), the IONPs became less uniform in both shape and size and the concave cubic morphology became less evident (Fig. S5b–c). Further increase in oleic acid concentration (4×) resulted in smaller and more spherical shaped IONPs (Fig. S5d), demonstrating that the concentration of oleic acid, which influences the chemical nature of the reaction mixture also plays an important role in forming the concave nanocube structure.

3.6 Oxidation of IONPs

All of the as-synthesized IONPs in Section 3.4.1 exhibit a wüstite (FeO) crystal phase from powder X-ray diffractometry (PXRD) analysis (Fig. 3a), which is in agreement with previously reported synthetic methods using iron oleate precursors [29, 35]. The FeO NPs were subsequently oxidized into the magnetite (Fe_3O_4) crystal phase through chemical oxidation (Fig. 3b). The obtained selected area electron diffraction (SAED) pattern further confirms the conversion of the IONPs to the Fe_3O_4 crystal phase after oxidation (Fig. 3c).

The magnetic properties of the Fe_3O_4 NPs synthesized from the different volume ratios of ODE:TOA were evaluated by measuring the field dependent magnetic hysteresis curves (Fig. 3d). From the SQUID magnetometry measurements, the smallest spherical NPs (synthesis vi) were evaluated to have the lowest Ms value at 49.2 emu/g, and the highest value at 86.4 emu/g for the concave cubic IONPs (synthesis i).

3.7 Relaxivity measurements

To study the MRI performance of the different IONPs synthesized using various ODE:TOA solvent ratios, the oxidized, oleic acid coated Fe_3O_4 NPs were first encapsulated in polysorbate-80 to facilitate water dispersity [23]. The average hydrodynamic radius of the concave nano-cubes was estimated from dynamic light scattering (DLS) measurements to be

117 nm. The T_2 relaxivities of the water-dispersed IONPs were evaluated using a 1.5 T 60 MHz Bruker minispec NMR relaxometer. An r_2 relaxivity value of 147.5 mM^{-1} s^{-1} was calculated for the spherical Fe_3O_4 NPs synthesized using 100% ODE solvent (Fig. 4), which is in agreement with previously reported values [5]. A significant increase in the r_2 relaxivity value was observed for the IONPs synthesized with larger TOA volume ratios. The IONPs with a concave cubic structure synthesized with 100 % TOA showed the highest r_2 relaxivity value of 862.2 mM^{-1} s^{-1}, which is about 6-fold higher than the r_2 measured for the spherical IONPs (Fig. 4). Moreover, the measured r_2 relaxivity value of the synthesized concave nanocube IONPs is significantly higher than the r_2 relaxivities of current clinically approved MRI and among the highest in previously reported IONP-based T_2 contrast agents [1, 6, 36]. The high r_2 relaxivity of the concave nanocubes can be attributed to its unique morphology and high Ms, which can generate a strong and expanded inhomogeneous magnetic field [6, 9]. Such strong inhomogeneous magnetic field surrounding a high-index faceted IONP can significantly impact the proton dephasing process, inducing a faster T_2 relaxation time and ultimately lead to better r_2 performance and enhanced T_2 MRI contrast.

To further investigate the effect of size and shape on the magnetic relaxivity of the synthesized IONPs, small and large sized spherical IONP samples were prepared. The r_2 relaxivity of the smaller sized nanosphere (12 nm) was compared to that of the larger nanosphere (40 nm), and a 2-fold enhancement in signal was observed with increase in NP size (Fig. S6). On the other hand, the concave nanocube sample (40 nm) with a similar size to the nanosphere showed 3× higher r_2 relaxivity, which supports the important role of shape in enhancing T_2 magnetic relaxivity (Fig.S6).

3.8 *In vivo* MRI experiments

To further assess the potential of the concave nanocubes as MRI contrast agents, the *in vivo* T_2*-weighted MR images of CD1-ICR mice injected with concave nanocube or spherical IONP contrast agents were compared using a 7 T pre-clinical Bruker Biospec MRI scanner. The water-dispersed IONP samples were injected at a dosage of0.3 mL at 2.5 mg Fe/kg. High resolution T_2*-weighted FLASH images (Fast Low Angle Shot) were obtained for each mouse at pre-injection (0 h) and 0.5 h post-injection. As shown in Fig. 5a, the injection of concave nanocube and spherical IONP samples both showed visible T_2*-weighted image contrast at the injection sites after 0.5 h of injection. Upon quantifying the signal-to-noise ratio (SNR) of the MRI image contrast acquired pre- and post-injection, the concave nanocubes showed over 2-fold significant improvement in image contrast compared to the spherical IONPs (Fig. 5b), indicating that the concave nanocubes with high r_2 value can lead to a significant darkening in the *in vivo* T_2*-weighted MRI images, therefore, it is a more effective T_2 contrast agent compared to the sphericalIONPs.

4 Discussion

Generally, the shape of NPs is defined by the preferential growth of one particular crystallographic direction over the others. One of the two extreme solvent conditions we studied in Section 3.4.1 is using ODE as the only solvent, in where we obtained spherical IONPs. ODE is known as a non-coordinating solvent [37], and thus, oleic acid acts as the

only ligand to yield the most energetically favorable structure with no preferential growth direction, the isotropic nanosphere shape.

Ligands/solvents with amine groups have been used in the syntheses of noble metal nanocrystals to induce high-index faceted structures due to their coordinating chemical interactions with the metal atoms [38]. In our study, we introduced the bulky TOA as the coordinating solvent instead of the non-coordinating ODE solvent into the thermal decomposition of the iron oleate precursor with optimum amount of oleic acid as the ligand, and the shape of the resulting NPs turned out to be concave cubic in morphology. Concave nanocubes or octopods are assumed to initiate their growth from truncated octahedral seeds and progress along the [111] direction at a faster rate compared to the [100] direction [39]. This proposed growth mechanism has been rationalized by Qiao et al. in a recent study, in which, they explained the formation of anisotropic IONPs as being a delicate balance between the chemical potentials (μ) of the reaction NP monomer units, i.e., the NP seeds, ($\mu_{m,i}$, chemical potential of i^{th}monomer), and the energetically different crystallographic planes of the IONPs ($\mu_{\{100\}}$,$\mu_{\{110\}}$, $\mu_{\{111\}}$, etc.) [39]. Specifically, as long as the monomer units satisfy the condition of $\mu_{\{100\}} > \mu_{\{110\}} > \mu_{m,i} > \mu_{\{111\}}$, the monomer units react promoting the growth along the {111} plane, which defines the concave cubic shape, while the growth along the {100} and {110} planes cease. Given that two types of monomer units with different potentials ($\mu_{m,\text{oleic acid}}$ and $\mu_{m,TOA}$) are used in our study, it isjudicious to assume that the monomer units with oleic acid molecules are capable to overcome the energy barrier along the {111} plane as it imposes less steric hindrance and can easily diffuse along the most crowded atomic plane compared to the monomer units associated with the bulky trioctylamine. According to our proposed mechanism, the monomer units surrounded with TOA preferentially bind to low-index facets such as the {100} plane and over growth with incoming monomers on those facets is restricted due to the steric hindrance posed by the TOA molecules. The selective binding of the two types of NP monomers allow us to propose the growth mechanism of concave IONPs as depicted in Fig. S7.

5 Conclusions

In conclusion, the role of a bulky coordinating solvent on the morphology evolution of concave nanocube IONPs was systematically investigated by increasing the volume ratio of the tertiary amine solvent. The binding ability and the bulky structure of TOA were demonstrated to be essential in the formation of the concave curvature on cubic IONPs. The concave nanocube IONPs synthesized from 100% TOA were evaluated to a have high T_2 relaxivity with about a 6-fold enhancement in transverse relaxivity (r_2) value and 2-fold enhancement in T_2*-weighted MR image contrast compared to spherical IONPs synthesized from a non-coordinating solvent. This study provides a simple alternative synthetic route towards the preparation of high relaxivity IONP-based contrast agents.

Supplementary Material

Refer to Web version on PubMed Central for supplementary material.

Acknowledgements

This work was supported by a NSF-CAREER Grant (DMR-1253358) from the Solid State and Materials Chemistry Program. Tilting TEM and SAED analyses on the concave nanocubes were performed with assistance from SCSAM at CWRU. The HRTEM data was obtained at the TEM facility at the Liquid Crystal Institute, Kent State University, supported by the Ohio Research Scholars Program Research Cluster on Surfaces in Advanced Materials. The authors thank the technical support of Dr. Min Gao for the HRTEM measurement.

References

1. Lee N, Choi Y, Lee Y, Park M, Moon WK, Choi SH, Hyeon T. Water-dispersible ferrimagnetic iron oxide nanocubes with extremely high r2 relaxivity for highly sensitive in vivo MRI of tumors. Nano Lett. 2012;12:3127–31. [PubMed: 22575047]
2. Lee N, Hyeon T. Designed synthesis of uniformly sized iron oxide nanoparticles for efficient magnetic resonance imaging contrast agents. Chem Soc Rev. 2012;41:2575–89. [PubMed: 22138852]
3. Todd T, Zhen Z, Tang W, Chen H, Wang G, Chuang YJ, Deaton K, Pan Z, Xie J. Iron oxide nanoparticle encapsulated diatoms for magnetic delivery of small molecules to tumors. Nanoscale. 2014;6:2073–6. [PubMed: 24424277]
4. Huang J, Wang L, Zhong X, Li Y, Yang L, Mao H. Facile nonhydrothermal synthesis of oligosaccharide coated sub-5 nm magnetic iron oxide nanoparticles with dual MRI contrast enhancement effects. J Mater Chem B. 2014;2:5344–51.
5. Yoo D, Lee JH, Shin TH, Cheon J. Theranostic magnetic nano-particles. Acc Chem Res. 2011;44:863–74. [PubMed: 21823593]
6. Zhao Z, Zhou Z, Bao J, Wang Z, Hu J, Chi X, Ni K, Wang R, Chen X, Chen Z, Gao J. Octapod Iron oxide nanoparticles as high performance T2 contrast agents for magnetic resonance imaging. Nat Commun. 2013;4:2266. [PubMed: 23903002]
7. Smolensky ED, Park HYE, Zhou Y, Rolla GA, Marjańska M, Botta M, Pierre VC. Scaling laws at the nanosize: the effect of particle size and shape on the magnetism and relaxivity of iron oxide nanoparticle contrast agents. J Mater Chem B. 2013; 1:2818–28. [PubMed: 23819021]
8. Roch A, Muller RN, Gillis P. Theory of proton relaxation induced by superparamagnetic particles. J Chem Phys. 1999;110:5403–11.
9. Zhou Z, Zhu X, Wu D, Chen Q, Huang D, Sun C, Xin J, Ni K, Gao J. Anisotropic shaped iron oxide nanostructures: controlled synthesis and proton relaxation shortening effects. Chem Mater. 2015;27:3505–15.
10. Situ SF, Samia ACS. Highly efficient antibacterial iron oxide@-carbon nanochains from wüstite precursor nanoparticles. ACS Appl Mater Interfaces. 2014;6:20154–63. [PubMed: 25347201]
11. Redl FX, Black CT, Papaefthymiou GC, Sandstrom RL, Yin M, Zeng H, Murray CB, O'Brien SP. Magnetic, electronic, and structural characterization of nonstoichiometric iron oxides at the nanoscale. J Am Chem Soc. 2004;126:14583–99. [PubMed: 15521779]
12. Park J, An KJ, Hwang Y, Park JG, Noh HJ, Kim JY, Park JH, Hwang NM, Hyeon T. Ultra-large-scale syntheses of mono-disperse nanocrystals. Nat Mater. 2004;3:891–5. [PubMed: 15568032]
13. Jun YW, Choi JS, Cheon J. Shape control of semiconductor and metal oxide nanocrystals through nonhydrolytic colloidal routes. Angew Chem Int Ed. 2006;45:3414–39.
14. Mohanty A, Garg N, Jin R. A universal approach to the synthesis of noble metal nanodendrites and their catalytic properties. Angew Chem Int Ed. 2010;49:4962–6.
15. Zeng H, Rice PM, Wang SX, Sun S. Shape-controlled synthesis and shape-induced texture of MnFe2O4 nanoparticles. J Am ChemSoc. 2004;126:11458–9.
16. Liang H, Jiang X, Qi Z, Chen W, Wu Z, Xu B, Wang Z, Mi J, LiQ. Hematite concave nanocubes and their superior catalytic activity for low temperature CO oxidation. Nanoscale. 2014;6:7199–203. [PubMed: 24871048]
17. Hofmann C, Rusakova I, Ould-Ely T, Prieto-Centurión D, Hartman KB, Kelly AT, Lüttge A, Whitmire KH. Shape control of new Fe_xO–Fe_3O_4 and $Fe_{1-y}Mn_yO$–$Fe_{3-z}Mn_zO_4$ nanostructures. Adv Funct Mater. 2008; 18:1661–7.

18. Bao L, Low WL, Jiang J, Ying JY. Colloidal synthesis of magnetic nanorods with tunable aspect ratios. J Mater Chem. 2012;22:7117–20.
19. Jin M, Zhang H, Xie Z, Xia Y. Palladium concave nanocubes with high-index facets and their enhanced catalytic properties. Angew Chem Int Ed. 2011;50:7850–4.
20. Shao Z, Zhu W, Wang H, Yang Q, Yang S, Liu X, Wang G. Controllable synthesis of concave nanocubes, right bipyramids, and 5-fold twinned nanorods of palladium and their enhanced electrocatalytic performance. J Phys Chem C. 2013;117: 14289–94.
21. Lee PY, Teng HS, Yeh CS. Preparation of superparamagnetic MnxFe1-xO nanoparticles from low-index-facet cubes to high-index-facet concave structures and their catalytic performance in aqueous solution. Nanoscale. 2013;5:7558–63. [PubMed: 23836257]
22. Kovalenko MV, Bodnarchuk MI, Lechner RT, Hesser G, Schäf-fler F, Heiss W. Fatty acid salts as stabilizers in size- and shape- controlled nanocrystal synthesis: the case of inverse spinel iron oxide. J Am Chem Soc. 2007;129:6352–3. [PubMed: 17472378]
23. Macher T, Totenhagen J, Sherwood J, Qin Y, Gurler D, Bolding MS, Bao Y. Ultrathin iron oxide nanowhiskers as positive contrast agents for magnetic resonance imaging. Adv Funct Mater. 2015;25:490–4.
24. Cozzoli PD, Snoeck E, Garcia MA, Giannini C, Guagliardi A, Cervellino A, Gozzo F, Hernando A, Achterhold K, Ciobanu N, Parak FG, Cingolani R, Manna L. Colloidal synthesis and characterization of tetrapod-shaped magnetic nanocrystals. Nano Lett. 2006;6:1966–72. [PubMed: 16968009]
25. Li Z, Ma Y, Qi L. Controlled synthesis of MnxFe1−xO concave nanocubes and highly branched cubic mesocrystals. CrystEngComm. 2014;16:600–8.
26. Palchoudhury S, Xu Y, Rushdi A, Holler RA, Bao Y. Controlled synthesis of iron oxide nanoplates and nanoflowers. Chem Commun. 2012;48:10499–501.
27. Douglas FJ, MacLaren DA, Tuna F, Holmes WM, Berry CC, Murrie M. Formation of octapod MnO nanoparticles with enhanced magnetic properties through kinetically controlled thermal decomposition of polynuclear manganese complexes. Nanoscale. 2014;6:172–6. [PubMed: 24220037]
28. Liao HG, Zherebetskyy D, Xin H, Czarnik C, Ercius P, Elmlund H, Pan M, Wang LW, Zheng H. Facet development during platinum nanocube growth. Science. 2014;345:916–9. [PubMed: 25146287]
29. Bronstein LM, Huang X, Retrum J, Schmucker A, Pink M, Stein BD, Dragnea B. Influence of iron oleate complex structure on iron oxide nanoparticle formation. Chem Mater. 2007;19:3624–32.
30. Ding X, Bao L, Jiang J, Gu H. Colloidal synthesis of ultrathin γ-Fe2O3 nanoplates. RSC Adv. 2014;4:9314–20.
31. Samia AC, Schlueter JA, Jiang JS, Bader SD, Qin CJ, Lin XM. Effect of ligand− metal interactions on the growth of transition-metal and alloy nanoparticles. Chem Mater. 2006;18:5203–12.
32. Nakamoto K. Infrared and Raman spectra of inorganic and coordination compounds, Part B: Applications in coordination, organometallic, and bioinorganic chemistry. 2nd edn New York: Wiley; 2009.
33. Lu Y, Miller JD. Carboxyl stretching vibrations of spontaneously adsorbed and LB-transferred calcium carboxylates as determined by FTIR internal reflection spectroscopy. J Colloid Interface Sci. 2002;256:41–52.
34. Tandon P, Förster G, Neubert R, Wartewig S. Phase transitions in oleic acid as studied by X-ray diffraction and FT-Raman spectroscopy. J Mol Struct. 2000;524:201–15.
35. Hufschmid R, Hamed A, Ferguson RM, Gonzales M, Teeman E, Brush LN, Browning ND, Krishnan KM. Synthesis of phase-pure and monodisperse iron oxide nanoparticles by thermal decomposition. Nanoscale. 2015;7:11142–54. [PubMed: 26059262]
36. Wang YXJ. Superparamagnetic iron oxide based MRI contrast agents: current status of clinical application. Quant Imaging Med Surg. 2011;1:35–40. [PubMed: 23256052]
37. Yu WW, Xiaogang P. Formation of high-quality CdS and other II–VI semiconductor nanocrystals in noncoordinating solvents: tunable reactivity of monomers. Angew Chem Int Ed. 2002;41:2368–71.

38. Huang X, Zhao Z, Fan J, Tan Y, Zheng N. Amine-assisted synthesis of concave polyhedral platinum nanocrystals having {411} high-index facets. J Am Chem Soc. 2011;133:4718–21. [PubMed: 21405136]

39. Qiao L, Fu Z, Li J, Ghosen J, Zeng M, Stebbins J, Prasad PN, Swihart MT. Standardizing size-and shape-controlled synthesis of monodisperse magnetite (Fe3O4) nanocrystals by identifying and exploiting effects of organic impurities. ACS Nano. 2017;11:6370–81. [PubMed: 28599110]

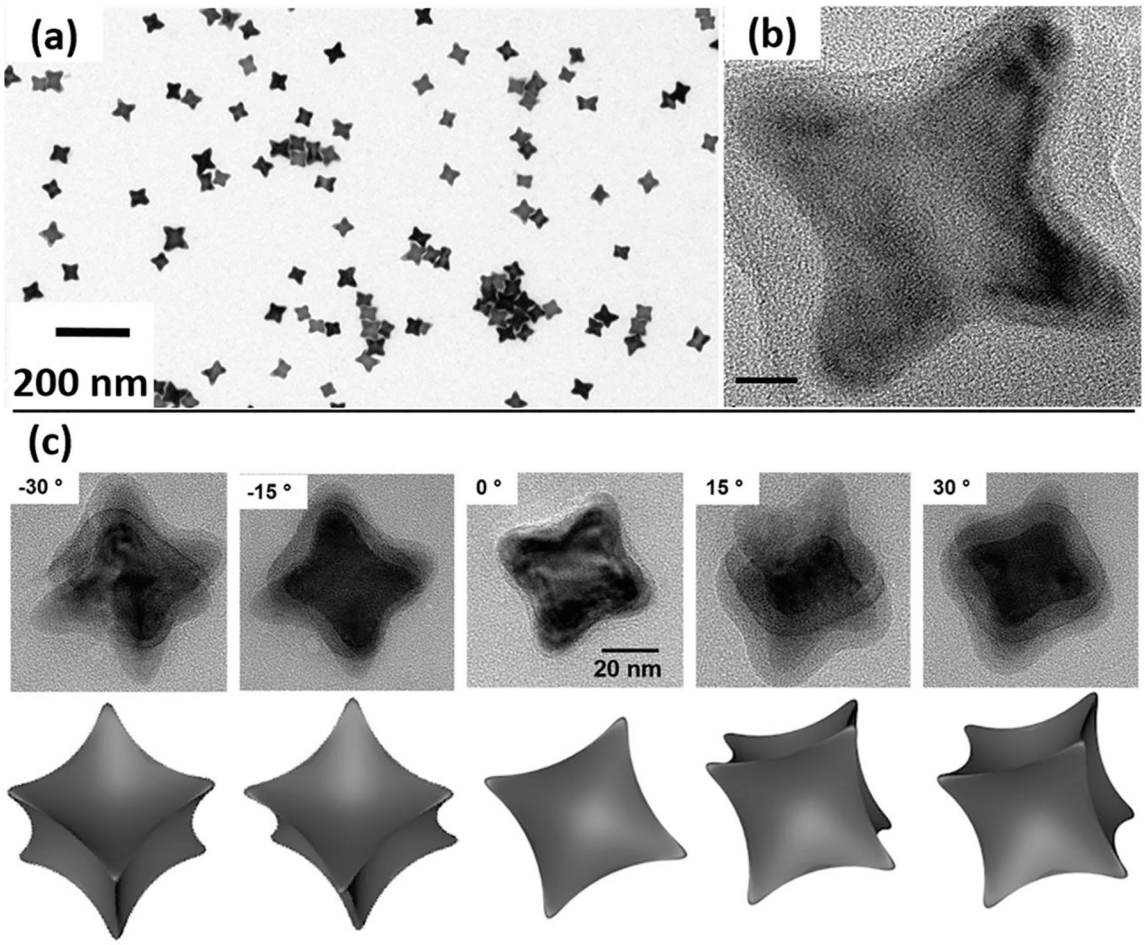

Fig. 1.

a Transmission electron microscopy (TEM) image of high-index faceted concave IONPs synthesized using a bulky coordinating ligand (TOA); **b** corresponding HRTEM image of the concave nanocube (scale bar, 10 nm). **c** Tilted TEM images of the concave nanocubes and the corresponding graphical representation of the rotation angles

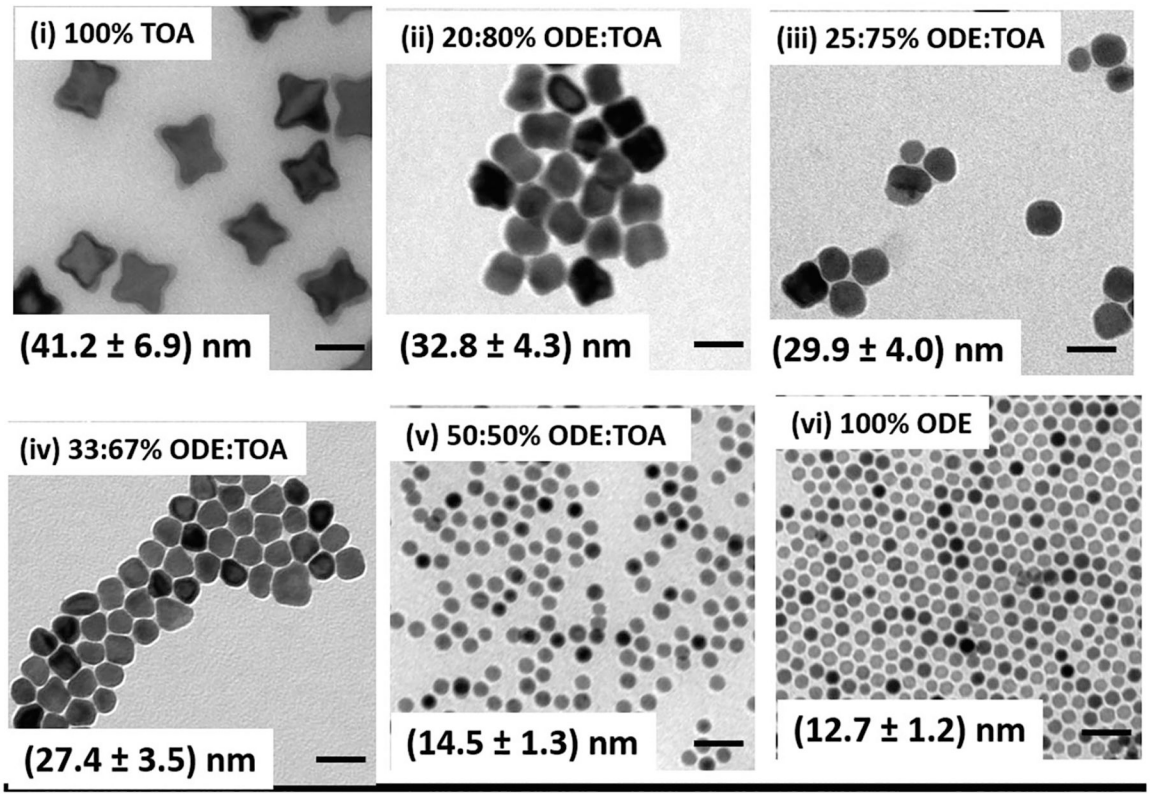

Fig. 2.

The NP morphology changes from anisotropic concave cubes to isotopic spheres upon introduction of a non-coordinating solvent, ODE. The scale bars represent 50 nm and the inset of each figure represents the average size of the NPs along with the solvent composition by the volume ratio (example: 20:80% ODE: TOA means 20% of the total solvent volume used during synthesis(ii) is ODE and so on)

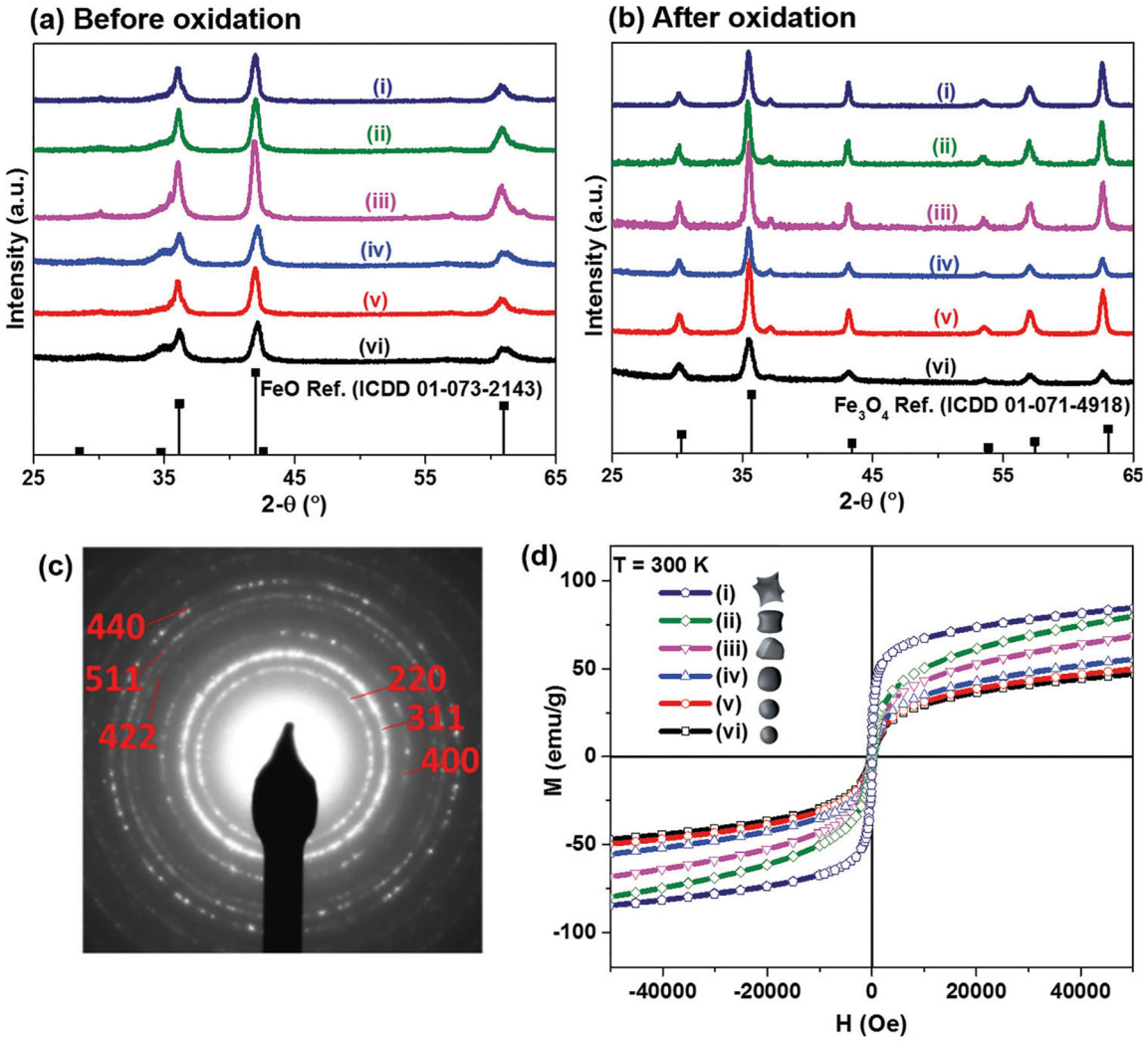

Fig. 3.

Powder x-ray diffraction patterns of the synthesized iron oxide nanoparticles obtained at different ODE:TOA solvent ratios: **a** before, **b** after chemical oxidation, **c** SAED of the oxidized concave cubes from synthesis (i), and **d** the corresponding field-dependent magnetization curves of the oxidized IONPs along with the corresponding graphical representations of the NPs

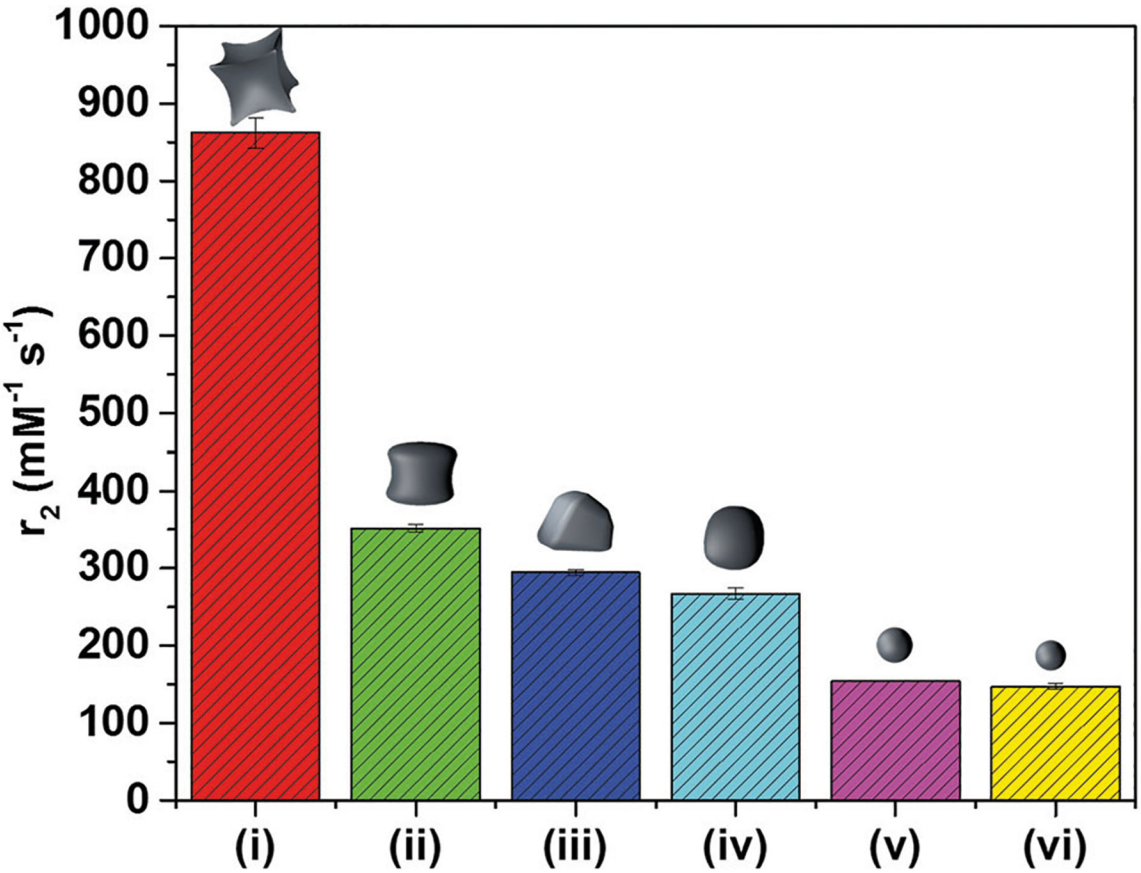

Fig. 4.

The transverse relaxivities (r_2) of the IONPs synthesized using different ODE and TOA solvent ratios; the average r_2 values were calculated from three replicate measurements

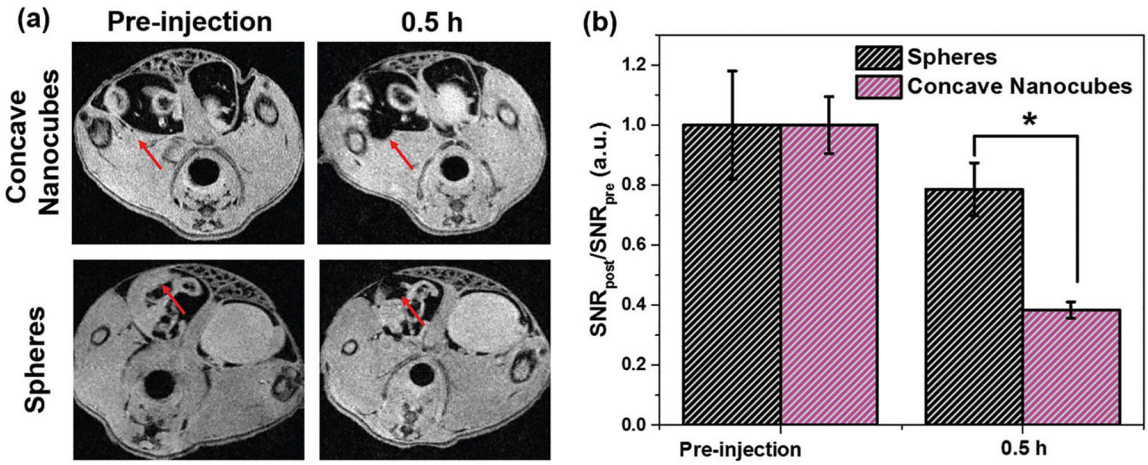

Fig. 5.

a *in vivo* MR images in transverse plane of CD1-ICR mice at 0 and 0.5 h after injection of concave nanocubes (upper) and spherical IONPs (lower) at a dosage of 2.5 mg Fe/kg, respectively. b The red arrows indicate the site of injection. The corresponding quantification of the MRI T_2*-contrast at the site of injection at 0.5 h post-injection; the asterisk indicates statistical significance with p-value less than 0.05 (color figure online)